

# Studying Intracellular Trafficking Pathways with Probabilistic Density Maps 20

Kristine Schauer\*, Tarn Duong<sup>†,‡</sup>, Carina S. Gomes-Santos\* and Bruno Goud\*

\**Molecular Mechanisms of Intracellular Transport, Unité Mixte de Recherche 144 Centre National de la Recherche Scientifique/Institut Curie, Paris cedex, France*

†*Theoretical and Applied Statistics Laboratory (LSTA), University Pierre and Marie Curie—Paris, Paris, France*

‡*Institute of Translational Neurosciences (IHU-A-ICM), Pitié-Salpêtrière Hospital, Paris, France*

## CHAPTER OUTLINE

<b>Introduction</b> .....	<b>326</b>
Intracellular Trafficking Pathways .....	326
Cell Confinement by Micropatterning Techniques .....	327
Probabilistic Density Mapping of Intracellular Compartments .....	329
Rationale .....	330
<b>20.1 Material and Methods</b> .....	<b>330</b>
20.1.1 Specific Materials (Excluding Generic Products) .....	331
20.1.2 Methods .....	331
20.1.2.1 Preparation of Micropatterns with Photolithography .....	331
20.1.2.2 Cell Seeding, Treatment, and Fixation .....	332
20.1.2.3 Immunolabeling (Optional) .....	333
20.1.2.4 Image Acquisition of Many Single Cells and Preanalysis ...	333
20.1.2.5 Density Mapping .....	334
<b>20.2 Results and Discussion</b> .....	<b>339</b>
<b>Summary</b> .....	<b>341</b>
<b>Acknowledgments</b> .....	<b>341</b>
<b>References</b> .....	<b>341</b>

## Abstract

The compartmentalization of cellular functions in complex membranous organelles is a key feature of eukaryotic cells. To cope with the enormous complexity of trafficking pathways that connect these compartments, new approaches need to be considered and introduced into the field of cell biology. We exploit the advantages of the “micropatterning technique,” which is to bring cells to adopt a highly reproducible

shape, and probabilistic density mapping, which quantifies spatial organization of trafficking compartments, to study regulatory mechanisms of intracellular trafficking. Here, we provide a protocol to analyze and quantify alterations in trafficking compartments upon cellular manipulation. We demonstrate how this approach can be employed to study the regulation of Rab6-labeled transport carriers by the cytoskeleton.

## INTRODUCTION

### Intracellular trafficking pathways

The endomembranous system of eukaryotic cells comprises several diverse organelles and tubular–vesicular transport carriers that are dynamic and highly interconnected by multiple routes. Classically, intracellular trafficking routes are divided into the secretory (or anterograde) pathway and the endocytic pathway. The endoplasmic reticulum (ER), the intermediate compartment (IC), the Golgi apparatus, and the *trans*-Golgi network (TGN) are considered to belong to the secretory pathway, whereas early (sorting) endosomes, late endosomes, lysosomes, and the endocytic recycling compartment (ERC) are most often classified to the endocytic pathway. Although functionally distinct, the secretory and endocytic pathways have parallel functions (Saraste & Goud, 2007). These include membrane and receptor recycling to maintain the integrity of the ER and the plasma membrane, respectively (Griffiths, Back, & Marsh, 1989; Martinez-Menarguez, Geuze, Slot, & Klumperman, 1999; Sannerud, Saraste, & Goud, 2003). Furthermore, their respective molecular machineries resemble each other (Bonifacino & Glick, 2004; Chia & Gleeson, 2011). Importantly, both pathways seem to partly overlap and to be intertwined at various branch points (Ellis, Potter, Cresawn, & Weisz, 2006; Lipschutz, Lingappa, & Mostov, 2003; Sannerud et al., 2003; Toikkanen, Miller, Soderlund, Jantti, & Keranen, 2003). For example, the ERC can sort molecules to the TGN (Wilcke et al., 2000) and the IC can contribute to endocytosis (Becker, Volchuk, & Rothman, 2005).

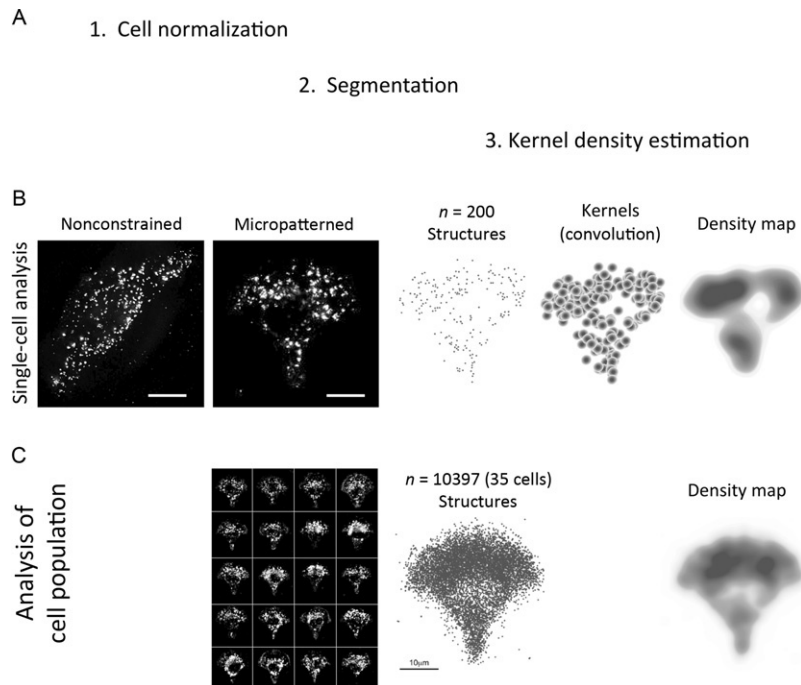
Although allowing the segregation of cellular processes, cellular compartmentalization demands an efficient and regulated communication among those compartments. Small GTPases of the Rab family are key regulators of intracellular trafficking, present in both secretory and endocytic pathways. There are over 60 members in human and they are highly conserved (found in all eukaryotes) (Pereira-Leal & Seabra, 2001). In their active form (GTP-bound), Rabs recruit a diverse range of effector proteins, such as molecular motors, lipid kinases, tethering factors, and scaffolding proteins, controlling the formation of transport carriers from donor membranes, their movement along cytoskeletal tracks, and their tethering/fusion with target membranes (Stenmark, 2009). Because Rab proteins are restricted to specific organelles or membrane microdomains, their presence not only regulates the trafficking throughout compartments but also defines their identity (Hutagalung &

Novick, 2011). Rab proteins are themselves under a strict spatiotemporal control by a complex network of proteins. Guanine nucleotide exchange factors (GEFs) stimulate the exchange GDP for GTP and thus activate Rab proteins and GTPase-activating proteins (GAPs) facilitate GTP hydrolysis and thus deactivate Rab proteins. Recent findings indicate that Rab proteins not only regulate individual transport steps but also function in a coordinated fashion, orchestrating sequential steps along transport pathways. An upstream Rab can recruit a GEF for a downstream Rab. In addition, a downstream Rab can recruit a GAP that will inactivate the upstream Rab (Rab GTPase cascades). Such a mechanism appears to be crucial to ensure continuity and directionality in membrane traffic (Jean & Kiger, 2012; Markgraf, Peplowska, & Ungermann, 2007).

The establishment and dynamics of trafficking routes and their regulation by Rab proteins are still not fully understood. Major challenges are the dynamic nature of trafficking events. Additionally, many trafficking compartments are spatially dispersed. Unlike compact structures such as the Golgi apparatus in mammalian cells and the ERC, endosomes and various transport carriers are present in high numbers and are located throughout the cells. This dispersed localization makes it very challenging to detect alterations in the compartment due to experimental manipulation or in pathological situations such as cancer development. To tackle these challenges, it is crucial to develop new quantitative approaches. Here, we present a method that allies cell normalization by micropatterning with probabilistic density mapping to quantitatively study intracellular trafficking pathways. Figure 20.1 outlines the probabilistic density-mapping procedure for a single cell and a cell population.

### Cell confinement by micropatterning techniques

The structured microenvironment of a tissue or organ imposes spatial restrictions on cells. These spatial cues force cells to take a specific, reproducible organization that is characteristic of tissues. Spatial cues have preponderant roles in a wide range of cellular functions, such as cell polarity, differentiation, division, and signaling (Gumbiner, 1996). Yet, classical *in vitro* cultured mammalian cells show strong cell-to-cell variations in morphology (Sigal et al., 2006). This heterogeneity has been attributed to unconstrained and dynamic cell shape, a consequence of the fact that cells move and constantly rearrange intracellular trafficking pathways. Furthermore, cells adapt to their local population context. Population size, local cell density, and position within a cellular islet have all been shown to determine cellular morphology and responsiveness (Snijder et al., 2009). The resulting heterogeneity hampers the understanding of the regulation of cellular trafficking pathways. In an attempt to transfer some of the *in situ* cues into classical cell culture conditions, various micro-fabricated substrates have been used in *in vitro* cell culture (Folch & Toner, 2000). Micropatterning technique comprises the fabrication of adhesive and nonadhesive regions that impose a defined geometry to cells upon adhesion. Throughout the years, the application of micropatterning technology has increased in cell biological studies, revealing important aspects of cell physiology. For instance, mesenchymal stem

**FIGURE 20.1**

Outline of the probabilistic density-mapping procedure exemplified for one single cell and cell populations. (A) Probabilistic density mapping of intracellular compartments requires cell normalization by micropatterning, extraction of point coordinates of imaged intracellular structures by segmentation, and kernel density estimation. (B) Example of this analysis for one single cell: the shape of the cell is first normalized by adhesion on a micropatterned shape (such as a crossbow), fluorescently labeled intracellular structures are transformed into point coordinates, and each of them is replaced by a Gaussian function (kernels) with mean zero and an optimized variance. Kernels are summed revealing the underlying density throughout the cell, where “red” corresponds to the most dense cellular regions. (C) Typically, several thousands of coordinates from several tens of normalized cells are used to calculate the density map of a population of cells.

cells plated on micropatterns differentiate either into adipocytes or osteoblasts, depending on the size and geometry of the pattern (McBeath, Pirone, Nelson, Bhadriraju, & Chen, 2004), revealing the importance of adhesive cues in cell fate. By applying controlled changes in micropattern geometry, it was also shown that cell adhesion determines the orientation of the mitotic spindle (Thery et al., 2005) and the orientation of the cell polarity axis (Thery et al., 2006).

These and other studies show that *in vitro* confinement of cell shape mimics the restriction of space that cells experience in body tissues (Gumbiner, 1996). Additionally, cell confinement on adhesive micropatterns of defined shapes normalizes

cellular shape, inner organization (Fig. 20.1B and C), and responsiveness to a given manipulation. Consequently, cell normalization allows the reduction of the number of analyzed cells required for statistically significant results. We showed that subtle drug effects on intracellular compartment were assessable using less than 20 micro-patterned cells (Duong, Goud, & Schauer, 2012; Schauer et al., 2010). Importantly, these effects could not be detected in conventionally grown unrestrained cells. Normalization additionally allows simplification and automatization of image analysis that is required for unbiased studies or high-throughput approaches.

### Probabilistic density mapping of intracellular compartments

A primary method for studying cellular function is to examine fluorescently labeled proteins after a given manipulation. Despite of the central role of morphology comparisons in cell biological approaches, few statistical tools are available that allow to quantify the similarity or difference of fluorescent images containing multivariate data. Because direct visualization of a large number of structures is not able to reveal details of the underlying spatial organization, statistical methods such as density mapping are required to visualize this organization (Fig. 20.1B and C). Density mapping is based on kernel density estimation, a set of advanced statistical techniques that are well suited to analyze multivariate data. Kernel estimators are convolutions, as each data point is blurred, in an inverse operation of the more widely known deconvolution, which takes a blurry image and sharpens it. This blurring or smoothing is a mathematical representation that an observed structure should represent not only itself but also other nearby structures that were not observed. The level of smoothing is the most important parameter to estimate optimally and has been the subject of much research, as it is also the most mathematically difficult to resolve (Duong & Hazelton, 2003, 2005). An oversmoothing leads to estimates that obscure the detailed structure of the data, whereas an undersmoothing leads to estimates that are too noisy with spurious data artifacts (Fig. 20.2). The mathematical complexity of kernel density estimators has thus historically limited their use beyond

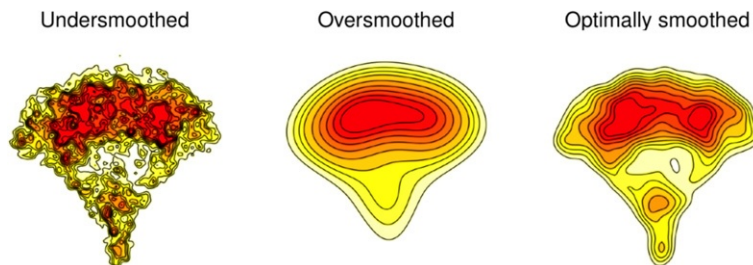


**FIGURE 20.2**

The smoothing parameter. The level of smoothing is the most important parameter to estimate optimally in a density map. An example is given of an oversmoothing that obscures the detailed structure of the data and an undersmoothing that leads to estimates that are too noisy with spurious data artifacts and optimal smoothing.

the statistical computing community. As a result, kernel density maps have been underused in the quantitative analysis of biological data in comparison to histogram maps, despite the well-documented evidence that kernel maps possess many favorable statistical properties over histograms (Simonoff, 1996; Wand & Jones, 1995). Fortunately, the growing availability of the user-friendly, open-source statistical computing software R, and especially the user-contributed add-on packages, has brought advanced statistical analysis to a larger pool of users.

In order to create spatial density maps of intracellular compartments, fluorescent microscopy images of endomembranes are segmented and the 3D spatial coordinates of the structures are extracted. Typically, several tens to several hundred structures of a specific compartment are extracted from each cell. Then, coordinates are replaced by kernels and summed, revealing the underlying density of a protein throughout the cell. The reproducible cellular orientation induced by the micropattern allows the collation of several tens (or more) of cells, thus resulting in an average density map for a population of analyzed cells. In addition to a visual summary, density maps are used to derive statistics for quantitative analysis of cell morphology. Probability contours indicate the regions of the highest local density/concentration of endomembranes (minimal regions for a given fixed proportion). They are useful because they admit an intuitive probabilistic interpretation, for example, the 50% probability contour defines the smallest region in which 50% of the endosomes are located. Applying density mapping to Rab6, we have found that secretory vesicles, labeled by this GTPase, preferentially localize at the adhesive edge of the cellular periphery and are trapped there by the actin cytoskeleton.

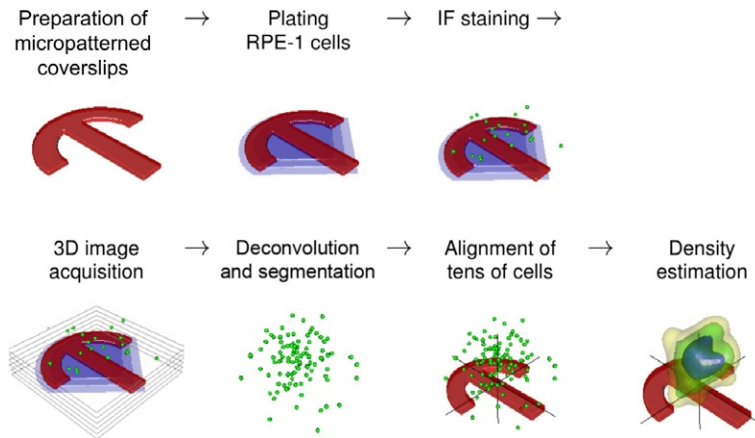
## Rationale

We will present how we exploit the advantages of the “micropatterning technique,” which is to bring cells to adopt a highly reproducible shape, and probabilistic density mapping that measures spatial organization of intracellular structures to quantitatively study the regulation of Rab6-labeled compartment by the cytoskeleton. Rab6 is the most abundant Rab in the Golgi apparatus and it is also present on vesicular post-Golgi transport carriers. It was found to be involved in several trafficking steps, both in the secretory and retrograde pathways (Goud & Akhmanova, 2012). Rab6-labeled transport carriers move along microtubules from the Golgi to the cell periphery, where some of them interact with cortical proteins and subsequently fuse with the plasma membrane. We assess how Rab6-labeled transport carriers are affected upon depolymerization of the cytoskeleton using nocodazole or cytochalasin D, which, respectively, disrupt microtubules or actin filaments.

---

## 20.1 MATERIAL AND METHODS

The experimental procedure is outlined in Fig. 20.3. It includes the preparation of micropatterned coverslips, cell plating, visualization of Rab6-labeled compartment, imaging of several tens of cells, image segmentation, alignment, and density mapping.

**FIGURE 20.3**

Schema of the experimental procedure. Micropatterned coverslips are prepared using photolithography. Cells are plated on micropatterns, structures of interest are visualized either by expressing fluorescently tagged proteins or indirect immunofluorescence, and 3D images are acquired. Images are deconvolved (if epifluorescence microscopy is used for 3D imaging) and positional information of fluorescently labeled structures is extracted from each single cell by segmentation analysis. Coordinates are aligned using the micropattern and the probability density map is calculated throughout the cell. To visualize the result, equally spaced probability contours are calculated that represent smallest areas in which a given percentage of structures are found.

### 20.1.1 Specific materials (excluding generic products)

- hTERT-RPE1 cells stably expressing EGFP-Rab6
- PLL(20)-g[3.5]-PEG(2) (PLL-g-PEG, poly-L-lysine-g-poly(ethyleneglycol), Surface Solutions), keep a stock solution at 1 mg/ml in 10 mM HEPES (pH 7.3) at 4 °C
- Photomask (Delta Mask)
- UVO Cleaner (Model 342-220, Jelight Company)
- Fibronectin
- Alexa-labeled fibrinogen (Amersham or Molecular Probes)
- 16% formaldehyde
- PBS/saponin/BSA (10 × stock solution: 20 g BSA, 5 g saponin, and 1 l PBS 10 ×).

### 20.1.2 Methods

#### 20.1.2.1 Preparation of micropatterns with photolithography

All steps have to be performed with the minimization of dust that will interfere with pattern quality. First, coverslips are cleaned by irradiation with UV light in the UV cleaner for 5 min. Coverslips are coated with PLL-g-PEG for 1 h, upside down in a wet chamber on parafilm, using 15  $\mu$ l (12 mm  $\varnothing$ ) or 30  $\mu$ l (18 mm  $\varnothing$ ) of 0.1 mg/ml PLL-g-PEG in 10 mM HEPES, pH 7.3. Coverslips are washed 2 × with PBS and

1 × with ddH<sub>2</sub>O using a multiwell plate and dried with the PEG-treated (hydrophobic) surface up. Before printing the micropatterns, the photomask is first rinsed with ddH<sub>2</sub>O and then with ethanol, dried with airflow, and irradiated with deep-UV light for 5 min. Then, 4 μl (12 mm Ø) or 6 μl (18 mm Ø) of ddH<sub>2</sub>O is pipetted on the photomask and coverslips are attached upside down on the mask using the capillary pressure. Extra water is removed with a tissue, until coverslips do not move anymore, and coverslips are covered with a big, thin glass plate or plastic film (e.g., old Western blot film). The photomask with attached coverslips is carefully installed upside down under the UV lamp of the UV cleaner and irradiated for 6 min. The UV light (30–33 mW/cm<sup>2</sup>, measured at 254 nm) passes through the micropattern shapes and changes the chemistry of the PLL-g-PEG layer (Azioune, Storch, Bornens, Thery, & Piel, 2009). Then, the photomask is removed from the UV cleaner and covered with plenteous water to remove the coverslips (coverslips will float). Coverslips are dried upright under a cover and stored for up to 4 weeks in multiwell plates until use.

#### **20.1.2.2 Cell seeding, treatment, and fixation**

Before cell plating, fibronectin is diluted to a final concentration of 50 μg/ml in ddH<sub>2</sub>O using 20 μl for a 12 mm Ø or 30 μl for a 18 mm Ø coverslip. To visualize micropatterns, Alexa-labeled fibrinogen is added at a final concentration of 5 μg/ml to the fibronectin solution. Coverslips are placed with the patterned surface on the mix and incubated for 1 h in the dark, in a wet chamber on parafilm. Afterward, they are incubated in plain DMEM/F12 medium/20 mM HEPES in a multiwell plate for 5 min, at 37 °C. Meanwhile, cells are trypsinized (60–80% confluence, grown for 3 days) and resuspended in full medium (DMEM/F12, 10% FBS, and 1% penicillin/streptomycin) in order to inactivate the trypsin. To obtain single cells, they are passed several times through the pipette and then added dropwise onto the coverslips (~300,000 cells). Cells are incubated for 5 min at room temperature (RT) (RPE-1 cells) or for 20 min in the incubator (HeLa cells). Because the attachment time varies between different cell lines, this parameter needs to be adjusted accordingly. Generally, we wait until the cells are attaching (1 cell per pattern) and the rest are still floating. Cells are then washed 3–10 × with plain medium/20 mM HEPES in order to remove all unbound cells. As the surface of coverslips is more hydrophobic than under classical cell culture conditions, some medium should always be left in the well to avoid drying out of the coverslips, which will cause cell death. The cells are incubated at 37 °C for 2–5 h for full spreading: RPE-1 cells require at least 2 h, and HeLa cells require at least 4 h. Typically, 25% of micropatterns are covered by a single cell, whereas the other 75% are either empty or covered by more than one cell. Once cells are spread, drugs are added directly into the medium. In the case of drugs that depolymerize actin filaments, only low concentrations are used to prevent cell rounding (e.g., 0.5 μM cytochalasin D). To depolymerize microtubules, cells are placed at 4 °C for 1 h prior to the addition of nocodazole (10 μM), a treatment that does not change cell shape. Cells are fixed with 16% formaldehyde that is added directly to the cells to obtain a final concentration of 4% and incubated for 15 min at room temperature.



### 20.1.2.3 Immunolabeling (optional)

After cell fixation, formaldehyde is quenched with 50 mM  $\text{NH}_4\text{Cl}$  for 5 min. Cells are washed 3  $\times$  with PBS and permeabilized with PBS/saponin/BSA for 20 min at RT. Coverslips are then incubated upside down in a drop (20  $\mu\text{l}$  for 12 mm  $\varnothing$  coverslips) containing the primary antibody in 2% BSA in PBS, in a wet chamber, in the dark for 45 min. Then, coverslips are washed 3  $\times$  with PBS and incubated in the same way with the secondary antibody followed by three washes with PBS and a short dip in  $\text{ddH}_2\text{O}$  (to remove PBS crystals). Coverslips are mounted with mowiol/DAPI mix (ca. 5  $\mu\text{l}$  for a 12 mm  $\varnothing$  coverslips) on an ethanol-cleaned slide and care is taken to avoid air bubbles or moving of the coverslip, which may deform micropatterned cells.

### 20.1.2.4 Image acquisition of many single cells and preanalysis

Images are acquired with any conventional microscope using a magnification that resolves the structures of interest. In the case of Rab6-labeled secretory vesicles, a 63  $\times$  or 100  $\times$  objective is required. For a typical analysis, several tens of cells (>20) are imaged; hence, microscopes with an automated stage are advantageous. To obtain 3D density maps,  $z$ -dimension series are acquired every 0.2–0.3  $\mu\text{m}$  and out-of-focus signals should be avoided (either by using confocal microscopy or performing deconvolution of epifluorescent images). To be able to process images in a batch mode, the images need to be numbered logically. For each cell, images are acquired for up to four fluorescence channels, including fluorescence staining of the micropattern (e.g., Cy5), the nucleus (e.g., Dapi), and the intracellular structures of interest (e.g., GFP). The nucleus staining is observed to verify that a single cell is analyzed, as several cells are frequently attached onto a single micropattern. Images of the structures of interest are segmented to extract their 3D spatial coordinates. This step translates the gray values of a camera chip into numbers that define intracellular structures. Several segmentation programs can be employed (Eliceiri et al., 2012), such as the “multidimensional image analysis” interface in MetaMorph (Universal Imaging Corporation) or “ParticleTracker.jar” in ImageJ (MOSAIC group, ETH, <http://www.mosaic.ethz.ch/Downloads/ParticleTracker>; Sbalzarini & Koumoutsakos, 2005). After segmentation, the coordinates (centroids) of all structures of interest from all cells are aligned using the micropattern. For this, coordinates of the center and the angle of rotation of the micropattern are measured, either automatically or manually. For automation, a macro can be established in ImageJ that chooses the most in-focus image of the 3D stack of fluorescently labeled patterns and applies the ImageJ plug-in “Hough Circles” to detect the center of a circle around the micropattern. Use a micropattern-shaped mask to determine the angle of rotation to orient cells in one direction. This preanalysis will provide a table containing (aligned) coordinates for each detected structure from several tens of cells. In supplementary data, you can find text files (.txt) containing coordinates from the small GTPase Rab6, monitored in 82 non-treated cells (Rab6NT82cells.txt), 50 cytochalasin D-treated cells (Rab6CD50cells.txt), and 47 nocodazole-treated cells (Rab6NZ47cells.txt), all normalized by micropatterning. These coordinate tables are required to calculate corresponding density maps for each condition.

### 20.1.2.5 Density mapping

The density estimation is performed using the `ks` library in R (R\_Development\_Core\_Team, 2013). R is a free program and can be downloaded and installed from the CRAN (Comprehensive R Archive Network) Website (<http://cran.r-project.org>). It is available on most platforms including Windows, Mac OS, and Unix/Linux. The procedure for installing R is already well documented on this site. To visualize density maps, the extension libraries `mvtnorm`, `rgl`, `miscd`, and `ks` are required that are available from the CRAN Website. Binary files are compiled versions of the source code and are the easier option. For those who have the ability and desire to compile the source code, this requires certain libraries to be installed, including a `gcc/fortran77` compiler, X11 Windows server, and PNG libraries.

#### 20.1.2.5.1 Program installation

1. Install the R base distribution from the R project Website <http://www.r-project.org> under the CRAN rubric, for example, `R-3.0.1.pkg` (for Macintosh) or `R-3.0.1-win32.exe` (for Windows).
2. Install the required extension packages. There are two main ways to do this.
  - a. Automatic: If the computer is connected to the Internet, packages can be installed directly using the Package Manager interface inside R. This is the preferred version as the most updated versions of the libraries will be automatically installed. Note that networks with a proxy cache or firewall may not allow for downloading in batch mode. Start R.
    - i. For Macintosh, select Packages & Data -> Package Installer. Make sure that At User Level is selected for Install Location. Choose the CRAN (binaries) under the Packages repository label. Click Get List.
    - ii. For Windows, select Packages -> Install Packages. Choose the closest CRAN mirror site. This will bring up a list of all extension packages.

Scroll down to select `ks`, and press Install. Repeat for the `rgl` and `misc3d` libraries.

- b. Manual: If the computer is not connected to the Internet, then the following packages must be downloaded using another computer from CRAN: `mvtnorm`, `rgl`, `miscd`, and `ks`. Go to the R project Website -> CRAN. Choose a CRAN mirror site. Click on the Contributed extension packages link. This will bring up the list of all contributed packages. Look for `mvtnorm`. Download the appropriate binary file (`.tgz` for Macintosh and `.zip` for Windows) to the desktop (or other desired location). Repeat for the `ks`, `rgl`, and `misc3d` libraries. Once all files have been downloaded, start R. To install these extension packages, perform the following:
  - i. For Macintosh, select Packages & Data -> Package Installer. Then select Local Binary Package under Packages Repository label. Select `mvtnorm` and press Install.
  - ii. For Windows, select Packages -> Install Packages from local zip files.

Install the extension packages in this order: `mvtnorm`, `ks`, `rgl`, and `misc3d`.

### 20.1.2.5.2 Density estimation

Three simple commands in R produce a kernel density map: (i) `Hpi()` calculates the optimal smoothing parameter for a density map, using a plug-in algorithm (Duong & Hazelton, 2003); (ii) `kde()` computes the density map; and (iii) `plot()` creates a graphical visualization of the density map.

```
smooth.param = Hpi(x=x)
density.map = kde(x=x, H=smooth.param)
plot(density.map)
```

The following procedure will calculate the density maps of the Rab6-labeled compartment using the table of (aligned) coordinates for each detected structure from several tens of cells obtained from the preanalysis. The text files, containing coordinates of Rab6-labeled structures under different experimental conditions and the R script required for the analysis, are provided in supplementary data. Save these data into a dedicated folder that will be the working directory. For other experimental conditions, coordinate tables of structures of interest need to be obtained and the R script needs to be adjusted (e.g., exchange `rab6.NT`) in order to calculate corresponding density maps.

1. Start R and load the `ks` library.

This can be done by selecting Packages & Data -> Package Manager (Macintosh) or Packages -> Load package (Windows), and then `ks`. Or it can be loaded by typing `library(ks)` into the command line window.

2. Choose the working directory in which txt files for analysis are located.

- (a) In Mac: ->Misc->Change Working Directory
- (b) In PC: ->File->Change dir ...

3. Open R script:

File->Open Document ...

4. Copy from R script the following script and paste in R Console:

```
## Load libraries
library(ks)
## Define calculation space

xlim2 <- c(-300,300)
ylim2 <- c(-300,300)
xlim <- c(-400,400)
ylim <- c(-400,400)
zlim <- c(-50,100)
lwd <- 3
xmin <- -c(400,400,100)
xmax <- c(400,400,100)
```

```

### Read in data files

rab6.NT <- read.table(file="Rab6NT82cells.txt", header=TRUE)
rab6.NZ <- read.table(file="Rab6NZ47cells.txt", header=TRUE)
rab6.CD <- read.table(file="Rab6CD50cells.txt", header=TRUE)

### Calculate density in 2D

H <- Hpi(rab6.NT[,1:2], binned=TRUE)
fhat2d.rab6.NT <- kde(x=rab6.NT[,1:2], H=H, xmin=xmin, xmax=xmax)
H <- Hpi(rab6.NZ[,1:2], binned=TRUE)
fhat2d.rab6.NZ <- kde(x=rab6.NZ[,1:2], H=H, xmin=xmin, xmax=xmax)
H <- Hpi(rab6.CD[,1:2], binned=TRUE)
fhat2d.rab6.CD <- kde(x=rab6.CD[,1:2], H=H, xmin=xmin, xmax=xmax)

### Calculate density in 3D

H <- Hpi(rab6.NT, binned=TRUE, bgridsize=rep(31,3))
fhat3d.rab6.NT <- kde(x=rab6.NT, H=H, xmin=xmin, xmax=xmax)
H <- Hpi(rab6.NZ, binned=TRUE, bgridsize=rep(31,3))
fhat3d.rab6.NZ <- kde(x=rab6.NZ, H=H, xmin=xmin, xmax=xmax)
H <- Hpi(rab6.CD, binned=TRUE, bgridsize=rep(31,3))
fhat3d.rab6.CD <- kde(x=rab6.CD, H=H, xmin=xmin, xmax=xmax)

### Create 2D plots
### 2D plotting functions

crossbow.3d <- array(0, dim=c(750, 750, 32))

crossbowt.3d <- crossbow.3d

contour.crossbow.2d <- function()
{
  x.cross <- tail(seq(-350, 350, length=751), -1)
  y.cross <- tail(seq(-350, 350, length=751), -1)
  contour(x.cross, y.cross, crossbowt.3d[, ,5], drawlabels=FALSE,
  lwd=4, col="grey", cex.lab=1.4, cex.axis=1.4, asp=1, xlim=xlim2,
  ylim=ylim2, xlab="x", ylab="y")
  lines(c(-100-10000/64.5, -100), c(-300,-300), lwd=lwd)
  text(-100-10000/64.5/2, -300, expression(10* $\mu$ *m), pos=3,
  cex=1.4)
}

### 2D plots

pdf(file="Rab6_NT.pdf")
par(mar=c(4,4,1,1), cex.main=1.4, lwd=lwd)
contour.crossbow.2d()
plot(fhat2d.rab6.NT, cont=25, col="red", add=TRUE, drawlabel=FALSE)
plot(fhat2d.rab6.NT, cont=50, col="orange", add=TRUE, drawlabel=FALSE)

```

```

plot(fhat2d.rab6.NT, cont=75, col="yellow", add=TRUE, drawlabel=FALSE)
legend("bottomright", title="Rab6 NT", legend=c("25%", "50%", "75%"),
      lwd=lwd,
      col=c("red", "orange", "yellow"), bty="n", cex=1.2)
dev.off()

pdf(file="Rab6_NZ.pdf")
par(mar=c(4,4,1,1), cex.main=1.4, lwd=lwd)
contour.crossbow.2d()
plot(fhat2d.rab6.NZ, cont=25, col="red", add=TRUE, drawlabel=FALSE)
plot(fhat2d.rab6.NZ, cont=50, col="orange", add=TRUE, drawlabel=FALSE)
plot(fhat2d.rab6.NZ, cont=75, col="yellow", add=TRUE, drawlabel=FALSE)
legend("bottomright", title="Rab6 NZ", legend=c("25%", "50%", "75%"),
      lwd=lwd,
      col=c("red", "orange", "yellow"), bty="n", cex=1.2)
dev.off()

pdf(file="Rab6_CD.pdf")
par(mar=c(4,4,1,1), cex.main=1.4, lwd=lwd)
contour.crossbow.2d()
plot(fhat2d.rab6.CD, cont=25, col="red", add=TRUE, drawlabel=FALSE)
plot(fhat2d.rab6.CD, cont=50, col="orange", add=TRUE, drawlabel=FALSE)
plot(fhat2d.rab6.CD, cont=75, col="yellow", add=TRUE, drawlabel=FALSE)
legend("bottomright", title="Rab6 CD", legend=c("25%", "50%", "75%"),
      lwd=lwd,
      col=c("red", "orange", "yellow"), bty="n", cex=1.2)
dev.off()

### Create 3D plots
### 3D plotting functions

vv3d <- function()
{
  par3d(userMatrix=matrix(c(0.87, -0.48, 0.04, 0, 0.10, 0.26, 0.96,
0, -0.48, -0.83, 0.29, 0, 0.00, 0.00, 0.00, 1), byrow=TRUE, ncol=4))
}

contour.crossbow.movie.3d <- function(add=TRUE, alpha=0.2, zoom=0.5)
{
  par3d(windowRect=c(0,0,500*16/9,500), zoom=zoom)
  ind <- seq(10, 750, by=10)
  x.cross <- tail(seq(-350, 350, length=751), -1)[ind]
  y.cross <- tail(seq(-350, 350, length=751), -1)[ind]
  z.cross <- seq(-2000/645*4, 2000/645*27, length=32)
  if (add)
    axis3d('z+', at=seq(0, 100, length=5), pos=c(-100, 100, NA))
  axis3d('x+', pos=c(NA, 100, 0))
}

```

```

axis3d('y+', pos=c(-100, NA, 0))
text3d(-120, 120, 80, "z")
text3d(0, 150, 0, "x")
text3d(-130, 0, 0, "y")
vv3d()
}

rotatez.movie.3d <- function(file="movie.mpeg", start=0, end=2*pi,
len=100, n=1)
{
  angle.step <- diff(seq(start, end, length=(n*len)))[1]
  for (i in 1:(n*len))
  {
    par3d(userMatrix=rotate3d(par3d())$userMatrix, angle.step, 0, 0, 1)
    snapshot3d(file=paste(file, sprintf("%03d", i), ".png", sep=""))
  }

  if (.Platform$OS.type=="unix")
  {
    #system(paste("convert -delay 10 ", file, "*.png -loop 0 ", file, sep=""))
  }
}

### 3d plots

plot(fhat3d.rab6.NT, col=c("yellow", "orange", "red"), xlim=xlim,
ylim=yylim, zlim=yylim, axes=FALSE, box=FALSE, asp=c(1,1,1), xlab="",
ylab="", zlab="")
contour.crossbow.movie.3d()
snapshot3d(file="Rab6_NT.png")

plot(fhat3d.rab6.NZ, col=c("yellow", "orange", "red"), xlim=xlim,
ylim=yylim, zlim=yylim, axes=FALSE, box=FALSE, asp=c(1,1,1), xlab="",
ylab="", zlab="")
contour.crossbow.movie.3d()
snapshot3d(file="Rab6_NZ.png")

plot(fhat3d.rab6.CD, col=c("yellow", "orange", "red"), xlim=xlim,
ylim=yylim, zlim=yylim, axes=FALSE, box=FALSE, asp=c(1,1,1), xlab="",
ylab="", zlab="")
contour.crossbow.movie.3d()
snapshot3d(file="Rab6_CD.png")

```

- 5.** Additional options to save a movie of the 3D density map and to save and load the calculated densities are provided by the following commands:

```

### 3d movies

rotatez.movie.3d()

```

```

## save densities
save(list=ls(pattern="fhat*"), file="Rab6.RData")

## reload calculated densities
load("Rab6.RData")

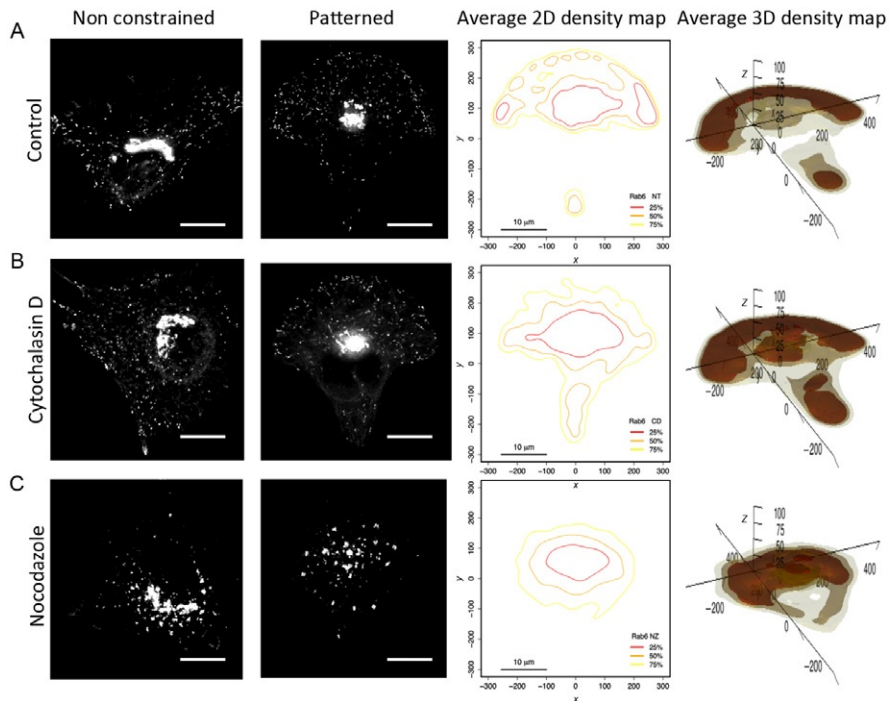
```

---

## 20.2 RESULTS AND DISCUSSION

To demonstrate the potential of our method to detect alterations in intracellular trafficking pathways, we analyze the Rab6-labeled compartment under different experimental conditions as an example. Whereas treatment with nocodazole gives rise to a strong phenotype that has been previously described (Grigoriev et al., 2007; Racine et al., 2007), treatment with cytochalasin D leads to subtle morphological changes on Rab6-labeled transport carriers. Nocodazole treatment fragments the Golgi and redistributes Rab6-labeled transport carriers from the cell periphery to the cell center, a phenotype easily assessable in nonrestricted and micropatterned cells (Fig. 20.4C). On the contrary, disruption of actin filaments does not show any strong effect in non-constrained cells or micropatterned cells as judged by visual estimation (Fig. 20.4B). Density mapping of the Rab6-labeled compartment in many normalized cells with disrupted actin shows however retraction of transport carriers from peripheral adhesive areas (Fig. 20.4B, right panel). This indicates that Rab6-labeled transport carriers are entrapped at the edge of the cell by actin filaments. Actin filaments are known to be organized close to the cell surface and to spread out trafficking vesicles (Nascimento, Roland, & Gelfand, 2003; Snider et al., 2004). To test for the significance of the difference between control cells and cytochalasin D-treated cells, density-based testing can be employed. Full automated testing can be performed using our multivariate two-sample test that is asymptotically normal under the null hypothesis allowing “black box” comparisons of multivariate data (Duong et al., 2012). The completely automatic testing procedure (including the parameter estimation and the computation of the test statistic and its  $P$ -value) is programmed in the `ks` library in R. Alternatively, resampling methods that compute the critical quantiles of the null distribution can be used requiring calibration for each data analysis at hand. For example, a distance function between pairs of points from different experimental conditions can be compared with a corresponding distance function from the same experimental condition (Schauer et al., 2010).

Alterations in intracellular trafficking are often revealed indirectly, mainly by the missorting of marker molecules, such as cargo proteins that are exchanged among the different intracellular compartments. Moreover, existing methods to study intracellular trafficking alterations do not provide a quantitative way to characterize the spatial distribution of the compartments, especially regarding those that are spatially dispersed, like transport carriers. By allying the micropatterning technique with probabilistic density maps, our method provides a direct and intuitive visualization of subcellular alterations in trafficking compartments. Therefore, it is extremely useful in the assignment of functional roles to trafficking components. In the future, it will be interesting to use this method to investigate whether patterned cells could be

**FIGURE 20.4**

Changes of Rab6-labeled compartment upon cytoskeletal disruption. (A) Rab6-labeled compartment in nontreated cells. Nonconstrained and micropatterned cells and the corresponding 2D and 3D density maps of 82 normalized cells are shown. (B) Rab6-labeled compartment upon cytochalasin D treatment in nonconstrained and micropatterned cells and the corresponding 2D and 3D density maps of 50 normalized cells. (C) Rab6-labeled compartment upon nocodazole treatment in nonconstrained and micropatterned cells and the corresponding 2D and 3D density maps of 47 normalized cells. The 25% (red), 50% (orange), and 75% (yellow) probability contours represent the smallest area in which a given percentage of Rab6-labeled structures are found: for example, the 50% probability contour defines the smallest area in which 50% of structures are located. Scale bars, 10 mm.

used as references to rapidly highlight pathological disorders, for example, during malignant development. Furthermore, this approach is a step towards the establishment of automated proceedings for high-content, high-throughput, phenotype-based screenings (Schauer et al., 2013). For instance, it could be used to identify scaffold, tether, or motor proteins that are regulated by a distinct Rab protein, for example, Rab6. As our method provides quantitative data from density-based analyses, we envision to use them for modeling approaches that could allow a better understanding of changes in intracellular organization of compartments in health and disease.



## SUMMARY

Crossing the border between different scientific disciplines is required to quantify changes in cellular morphology in a robust, unbiased, and automated manner in high throughput. We present how an advanced mathematical method, density estimation, is employed to move to quantitative cell biology, allowing detailed analysis of complex cellular behavior.

## Acknowledgments

We thank Laura Picas and Lena Oesterlin for critical reading of the chapter. K. S. received funding from the Fondation pour la Recherche Médicale en France and Association pour la Recherche sur le Cancer. T. D. received funding from the program “Investissements d’avenir” ANR-10-IAIHU-06. C. S. G. S. is supported by the Marie Curie Fellowship PIEF-GA-2011-299756. This project was further supported by grants from Agence Nationale de la Recherche (#2010 BLAN 122902), the Centre National de la Recherche Scientifique, and Institut Curie.

*Conflict of interest statement:* A patent (PCT n° EP2012/064239) has been filed on the density-based two-sample test.

## References

- Azioune, A., Storch, M., Bornens, M., They, M., & Piel, M. (2009). Simple and rapid process for single cell micro-patterning. *Lab on a Chip*, 9, 1640–1642.
- Becker, T., Volchuk, A., & Rothman, J. E. (2005). Differential use of endoplasmic reticulum membrane for phagocytosis in J774 macrophages. *Proceedings of the National Academy of Sciences of the United States of America*, 102, 4022–4026.
- Bonifacino, J. S., & Glick, B. S. (2004). The mechanisms of vesicle budding and fusion. *Cell*, 116, 153–166.
- Chia, P. Z., & Gleeson, P. A. (2011). The regulation of endosome-to-Golgi retrograde transport by tethers and scaffolds. *Traffic*, 12, 939–947.
- Duong, T., Goud, B., & Schauer, K. (2012). Closed-form density-based framework for automatic detection of cellular morphology changes. *Proceedings of the National Academy of Sciences of the United States of America*, 109, 8382–8387.
- Duong, T., & Hazelton, M. L. (2003). Plug-in bandwidth matrices for bivariate kernel density estimations. *Journal of Nonparametric Statistics*, 17, 17–30.
- Duong, T., & Hazelton, M. L. (2005). Cross-validation bandwidth matrices for multivariate kernel density estimation. *Scandinavian Journal of Statistics*, 32, 485–506.
- Eliceiri, K. W., Berthold, M. R., Goldberg, I. G., Ibanez, L., Manjunath, B. S., Martone, M. E., et al. (2012). Biological imaging software tools. *Nature Methods*, 9, 697–710.
- Ellis, M. A., Potter, B. A., Cresawn, K. O., & Weisz, O. A. (2006). Polarized biosynthetic traffic in renal epithelial cells: Sorting, sorting, everywhere. *American Journal of Physiology Renal Physiology*, 291, F707–F713.
- Folch, A., & Toner, M. (2000). Microengineering of cellular interactions. *Annual Review of Biomedical Engineering*, 2, 227–256.
- Goud, B., & Akhmanova, A. (2012). *Rab6 GTPase*. Danvers: Bentham Science.

- Griffiths, G., Back, R., & Marsh, M. (1989). A quantitative analysis of the endocytic pathway in baby hamster kidney cells. *The Journal of Cell Biology*, *109*, 2703–2720.
- Grigoriev, I., Splinter, D., Keijzer, N., Wulf, P. S., Demmers, J., Ohtsuka, T., et al. (2007). Rab6 regulates transport and targeting of exocytotic carriers. *Developmental Cell*, *13*, 305–314.
- Gumbiner, B. M. (1996). Cell adhesion: The molecular basis of tissue architecture and morphogenesis. *Cell*, *84*, 345–357.
- Hutagalung, A. H., & Novick, P. J. (2011). Role of Rab GTPases in membrane traffic and cell physiology. *Physiological Reviews*, *91*, 119–149.
- Jean, S., & Kiger, A. A. (2012). Coordination between RAB GTPase and phosphoinositide regulation and functions. *Nature Reviews Molecular Cell Biology*, *13*, 463–470.
- Lipschutz, J. H., Lingappa, V. R., & Mostov, K. E. (2003). The exocyst affects protein synthesis by acting on the translocation machinery of the endoplasmic reticulum. *Journal of Biological Chemistry*, *278*, 20954–20960.
- Markgraf, D. F., Peplowska, K., & Ungermann, C. (2007). Rab cascades and tethering factors in the endomembrane system. *FEBS Letters*, *581*, 2125–2130.
- Martinez-Menarguez, J. A., Geuze, H. J., Slot, J. W., & Klumperman, J. (1999). Vesicular tubular clusters between the ER and Golgi mediate concentration of soluble secretory proteins by exclusion from COPI-coated vesicles. *Cell*, *98*, 81–90.
- McBeath, R., Pirone, D. M., Nelson, C. M., Bhadriraju, K., & Chen, C. S. (2004). Cell shape, cytoskeletal tension, and RhoA regulate stem cell lineage commitment. *Developmental Cell*, *6*, 483–495.
- Nascimento, A. A., Roland, J. T., & Gelfand, V. I. (2003). Pigment cells: A model for the study of organelle transport. *Annual Review of Cell and Developmental Biology*, *19*, 469–491.
- Pereira-Leal, J. B., & Seabra, M. C. (2001). Evolution of the Rab family of small GTP-binding proteins. *Journal of Molecular Biology*, *313*, 889–901.
- R\_Development\_Core\_Team (2013). *R: A language and environment for statistical computing*. Vienna, Austria: R Foundation for Statistical Computing.
- Racine, V., Sachse, M., Salamero, J., Fraissier, V., Trubuil, A., & Sibarita, J. B. (2007). Visualization and quantification of vesicle trafficking on a three-dimensional cytoskeleton network in living cells. *Journal of Microscopy*, *225*, 214–228.
- Sannerud, R., Saraste, J., & Goud, B. (2003). Retrograde traffic in the biosynthetic-secretory route: Pathways and machinery. *Current Opinion in Cell Biology*, *15*, 438–445.
- Saraste, J., & Goud, B. (2007). Functional symmetry of endomembranes. *Molecular Biology of the Cell*, *18*, 1430–1436.
- Sbalzarini, I. F., & Koumoutsakos, P. (2005). Feature point tracking and trajectory analysis for video imaging in cell biology. *Journal of Structural Biology*, *151*, 182–195.
- Schauer, K., Duong, T., Bleakley, K., Bardin, S., Bornens, M., & Goud, B. (2010). Probabilistic density maps to study global endomembrane organization. *Nature Methods*, *7*, 560–566.
- Schauer, K., Grossier, J.-P., Duong, T., Chapuis, V., Degot, S., Lescure, A., et al. (2013). A novel “Organelle Map” framework for high-content cell morphology analysis in high-throughput. *Journal of Biomolecular Screening*, 2013, Aug 16. [Epub ahead of print].
- Sigal, A., Milo, R., Cohen, A., Geva-Zatorsky, N., Klein, Y., Liron, Y., et al. (2006). Variability and memory of protein levels in human cells. *Nature*, *444*, 643–646.
- Simonoff, J. S. (1996). *Smoothing methods in statistics*. New York: Springer-Verlag.
- Snider, J., Lin, F., Zahedi, N., Rodionov, V., Yu, C. C., & Gross, S. P. (2004). Intracellular actin-based transport: How far you go depends on how often you switch. *Proceedings of the National Academy of Sciences of the United States of America*, *101*, 13204–13209.

- Snijder, B., Sacher, R., Ramo, P., Damm, E. M., Liberali, P., & Pelkmans, L. (2009). Population context determines cell-to-cell variability in endocytosis and virus infection. *Nature*, *461*, 520–523.
- Stenmark, H. (2009). Rab GTPases as coordinators of vesicle traffic. *Nature Reviews Molecular Cell Biology*, *10*, 513–525.
- Thery, M., Racine, V., Pepin, A., Piel, M., Chen, Y., Sibarita, J. B., et al. (2005). The extracellular matrix guides the orientation of the cell division axis. *Nature Cell Biology*, *7*, 947–953.
- Thery, M., Racine, V., Piel, M., Pepin, A., Dimitrov, A., Chen, Y., et al. (2006). Anisotropy of cell adhesive microenvironment governs cell internal organization and orientation of polarity. *Proceedings of the National Academy of Sciences of the United States of America*, *103*, 19771–19776.
- Toikkanen, J. H., Miller, K. J., Soderlund, H., Jantti, J., & Keranen, S. (2003). The beta subunit of the Sec61p endoplasmic reticulum translocon interacts with the exocyst complex in *Saccharomyces cerevisiae*. *Journal of Biological Chemistry*, *278*, 20946–20953.
- Wand, M. P., & Jones, M. C. (1995). *Kernel smoothing*. London: Chapman & Hall/CRC.
- Wilcke, M., Johannes, L., Galli, T., Mayau, V., Goud, B., & Salamero, J. (2000). Rab11 regulates the compartmentalization of early endosomes required for efficient transport from early endosomes to the trans-golgi network. *The Journal of Cell Biology*, *151*, 1207–1220.